# Modeling the radiometric imaging process of weld pool

*Liang Zhimin, Shi Kangning, Wang Zhijiang and Wang Dianlong*
梁志敏, 石康柠, 王志江, 汪殿龙 *

***Abstract*** *In the vision monitoring or controlling the arc welding process, it is a prerequisite to get a clear image of weld pool. However, the disturbance of arc radiation makes imaging of weld pool difficult and optical filters are usually used to improve the image quality. In this paper, a radiometric imaging model is established to investigate the influence of the filter on the image quality of the weld pool, in which the spectral distribution of weld pool radiation, the spectral transmittance of the filter, the spectral sensitivity of the camera are all considered. With the proposed model, the influence of the factors on weld pool imaging can be inferred and the selection of optical filters is discussed.*

**Key words** radiometric modeling, weld pool imaging, visual sensing

## 0 Introduction

Skilled welders use vision to observe the weld pool and make judgements about the welding process and adjust the welding parameters accordingly. This indicates that weld pool surface contains significant information to determine the weld quality. For an automatic arc welding, a vision sensor is often used to emulate skilled welder's eyes to capture the image of weld pool and extract information about the quality of weld. Further, vision monitoring of an arc welding process has become an attractive tool to elucidate arc welding phenomena, such as droplet transfer, fluid flow on the weld pool surface and so on[1-2].

However, the interference of the extremely strong light in an arc welding process makes it difficult to acquire satisfied images of weld pool which contain enough information to be extracted in the following image analysis step. To reduce the disturbance of the strong arc, several techniques have been proposed. According to whether an auxiliary light source is used, these techniques can be classified into active methods and passive methods. Although the active vision methods using structured light pattern have obtained preliminary results[3-5]. However, the use of high speed camera and the auxiliary light source limited its industrial application.

It is an attractive idea from both academic and industrial point of view to develop a passive vision system for arc welding monitoring without using any auxiliary light source. In this technique, a narrow band optical filter which has the function similar to the welding shield glass used by human welder is often used to reduce disturbance of the intense arc. However, the optical filters selected in different investigations are different. For example, narrow band filters centered at visible range[6-8], infrared range[8-10] had been used for arc welding monitoring. Long pass filter was also employed[8]. Generally, spectral analysis of arc and weld pool is often conducted to select a spectral window for optical filter where the radiation of arc is relatively low and no characteristic line spectrum of arc exists. But the intensity of welding arc changes dramatically with welding conditions, such as welding current, base metal, shielding gas, welding wire, metal transfer and so on, which makes the spectral analysis results differ a lot. Further, the spectral sensitivities of different cameras are also different. All the above causes that the selection of optical filters has not yet reached a uniform understanding.

In a previous work, an experimental comparison of imaging weld pool of P-GMAW has been made using filters

* Liang Zhimin, Shi Kangning and Wang Dianlong, School of Material Science and Technology, Hebei University of Science and Technology, Shijiazhuang, 050018. Wang Zhijiang, School of Material Science and Technology, Tianjin University, Tianjin, 300072. Liang Zhimin, Corresponding author, E-mail: lianghebust@163.com

with different center wavelength[11]. In this study, a radiometric image forming model is proposed for weld pool monitoring by considering the weld pool radiation, the spectral transmittance of the filter and the spectral sensitivity of the camera. To validate the model, images of weld pool in P-GMAW have been captured with a series of narrow band filters centered from ultraviolet light to infrared light. The characteristic of images taken by a variety of filters are analyzed, and comparison of the image brightness predicted by the model and measured in experiment is also made to verify the effectiveness of the proposed model.

## 1 Modeling of radiometric imaging

In arc welding process monitoring, the image of weld pool in a 3D scene is a 2D array brightness (or color of red, green, blue) values. The geometric relation between the point in the 3D scene and its projected position in the 2D image is well described by a proper camera model, such as pinhole model, while the radiometric relation between the actual scene brightness and the image brightness is complicated. To discuss radiometric image forming process, some basic concept should be clarified. In radiometry, the intensity of light is defined by the term of radiance, which is the power of energy traveling at some point in a specified direction, per unit area perpendicular to the travel direction, per unit solid angle. The power of radiant energy falling on a plane is called the image irradiance, which is defined as the incident flux divided by the area of surface patch[12].

A simple radiometric imaging system of weld pool is shown in Fig. 1. The whole process can be divided into three steps. First, the light is emitted by thermal radiation of the weld pool surface and is transmitted into the hemisphere space with a intensity of $L(\lambda)$. Second, a small fraction of the light emitted from a small area patch $dA_o$ on weld pool surface passes the filter with a spectral transmittance curve $F(\lambda)$ and lens system, and is projected into some area $dA_i$ on the image plane. The image irradiance $E(\lambda)$ can be calculated in this step. Finally, all the lights on image plane are usually picked up by an imaging sensor with a spectral sensitivity of $S(\lambda)$, integrated for the duration of exposure time, and then passed to a set of sensing amplifiers. So an image of 2D array of brightness values (or color values) is obtained. These steps are denoted in Fig. 1 by Ⅰ, Ⅱ and Ⅲ, which will be discussed in the following.

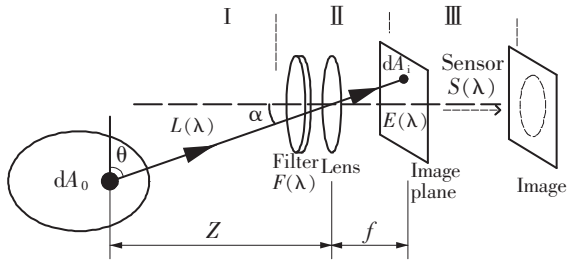


**Fig. 1 Radiometric imaging process**

### 1.1 Thermal radiation of weld pool

All bodies above zero degree (in K) radiate thermal energy. The emitted radiance per unit wavelength or spectral radiance of a black body is given by the Planck radiation law[13]:

$$L(\lambda, T) = \frac{2C_1}{\lambda^5 (e^{C_2/(\lambda T)} - 1)} \tag{1}$$

where $\lambda$ is the wavelength, $T$ is the absolute temperature and the constant $C_1$ equals to $hc_0^2$ and the constant $C_2$ equals to $hc_0/k$, where $h$ is Planck's constant and $k$ is the Boltzmann constant.

A real body, such as the weld pool, emits only a fraction of what a black body emits at any given temperature. However, the spectral analysis of thermal radiation from the weld pool in experiment is tend to well correspond with the calculated results by Planck's Law for blackbody radiation[10].

### 1.2 Step from scene radiance to image irradiance

In this step, the light passes through the optical filter and the lens system. The filter filtrate the light of $L(\lambda)$ and the aperture of lens restricts the solid angle of light transmitting. Optical filters are characterized quantitatively by spectral transmittance $F(\lambda)$, which is defined as the ratio of the transmitted radiant flux $(\Phi_\lambda)_t$ to the incident radiant flux $(\Phi_\lambda)_i$:

$$F(\lambda) = \frac{(\Phi_\lambda)_t}{(\Phi_\lambda)_i} \tag{2}$$

For a neutral density filter, the spectral transmittance is constant, so it attenuates light without discrimination of the wavelength. An interference narrow band filter is used to isolate and transmit a narrow wavelength range with high transmission and block all other wavelengths above or below the wavelength through absorption and/or reflection. A typical spectral transmittance curve for a narrow band filter is shown in Fig. 2. The most important properties of narrow band pass filters can be defined by the following values: maximum spectral transmittance within the pass band $\tau_{\max}$, center wavelength (CWL) of the pass band $\lambda_c$, full width at half maximum (FWHM)—the bandwidth at 50% of the maximum transmittance $\Delta\lambda$ and the blocking range—the spectral region in which the filter does not transmit. The transmittance $F(\lambda)$ can be approximated by Gaussian function. The wavelength outside the range $[\lambda_c - \Delta\lambda \quad \lambda_c + \Delta\lambda]$ can be viewed as the blocking range, the spectral transmittance function $F_{NB}(\lambda)$ for narrow band filter can be written as:

$$F_{NB}(\lambda) = \begin{cases} \tau_{\max} e^{-\frac{(\lambda-\lambda_c)^2}{\Delta\lambda^2/4\ln 2}} & |\lambda - \lambda_c| \leqslant \Delta\lambda \\ 0 & |\lambda - \lambda_c| > \Delta\lambda \end{cases} \tag{3}$$

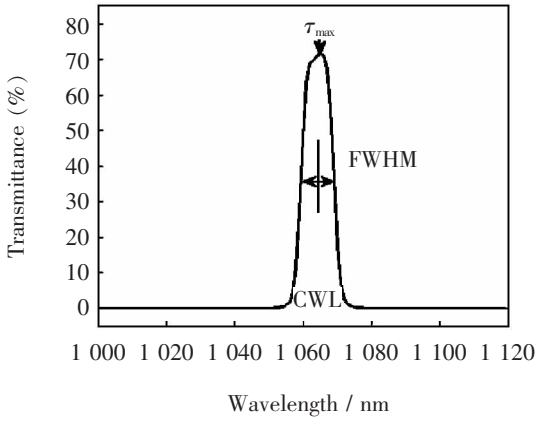


**Fig. 2 Spectral transmittance curve for a narrow band filter of 1 064 nm**

The light which has transmitted the filter will pass through the lens system before reaching the image plane. It is assumed that there is no power loss in the lens, but the aperture of lens restricts the solid angle of light transmitting. As shown in Fig. 1, the angle $\theta$ is between the normal on the surface and the line to the entrance aperture nodal point, while $\alpha$ is the angle between this line and the optical axis. The entrance aperture is a circle of diameter $D$. If the system is well focused, all those light rays originated from the same patch will fall on the same area in image plane. Thus the spectral image irradiance $E(\lambda)$ passing through the aperture originating from the patch of area $dA_o$ on the weld pool is determined as:

$$E(\lambda) = \frac{F(\lambda)\int_\Omega L(\lambda)\,dA_0\cos\theta d\Omega}{aA_i} \tag{4}$$

where $\Omega$ is the projected solid angle subtended by the entrance aperture of the lens as seen from the surface patch. If the diameter $D$ of aperture is small relative to its distance from the object, the radiance $L(\lambda)$ is constant. The solid angle $\Omega$ is approximately equal to the foreshortened area divided by the distance squared:

$$\Omega = \frac{(\pi D^2/4)\cos\alpha}{Z^2} \tag{5}$$

Further, the solid angle of $dA_0$ and $dA_i$ is equaled, which can be expressed:

$$\frac{dA_0\cos\theta}{Z^2} = \frac{dA_i\cos^3\alpha}{f^2} \tag{6}$$

Substituting equation (5) and equation (6) in equation (4), $E(\lambda)$ is rewritten as:

$$E(\lambda) = \left(\frac{\pi}{4}\right)\left(\frac{D}{f}\right)^2\cos^4\alpha L(\lambda)F(\lambda)$$

In optics, the $f$-number $f_{num}$ (sometimes called focal ratio, f-ratio or relative aperture) is equal to the focal length of the lens divided by the effective diameter of the lens, i. e.:

$$f_{num} = \frac{f}{D}$$

Thus, the image irradiance $E(\lambda)$ as a function of the object spectral radiance $L(\lambda)$, filter's spectral transmittance $F(\lambda)$ and the relative aperture $f_{num}$ is given as:

$$E(\lambda) = \left(\frac{\pi}{4}\right)\cos^4\alpha\left(\frac{1}{f_{num}}\right)^2 L(\lambda)F(\lambda) \tag{7}$$

### 1.3 Step from image irradiance to image brightness

After the light falling on the image plane as image irradiance, an imaging sensor (or an array of sensors) converts the received radiation into an electrical signal that is subsequently sampled and digitized to form a digital image as an array of digital numbers known as brightness or color value. Most cameras introduce nonlinear mapping between the image brightness and the image irradiance, which is related by the camera spectral sensitivity $S(\lambda)$. For precise measurement of the spectral sensitivity of a camera, a monochromator is used to converts the continuous spectrum of a xenon or tungsten lamp into a set of equally spaced monochrome wavelengths with a desired interval. The monochromatic light is then measured with both the camera and a spectroradiometer. The spectral sensitivity of the camera $S(\lambda)$ is determined as the ratio of the observed image intensity value and the measured radiance at each of the sampling wavelengths[14]. So considering the exposure time, the brightness $G(x)$ of a pixel $x$ in image can be given as:

$$G(x) = \int_t\int_A\int_\lambda S(\lambda)E(\lambda)\,d\lambda\,dA\,dt + \xi$$

where $A$ is the area of pixel, $t$ is the exposure time and $\xi$ is the noise.

Substituting equation (7) of image irradiance $E(\lambda)$ and assuming that the radiance $L(\lambda)$ does not change within exposure time $t$ and pixel area $A$, the brightness value $G(x)$ of the pixel is rewritten as:

$$G(x) = \left(\frac{\pi}{4}\right)\left(\frac{1}{f_{num}}\right)^2\cos^4\alpha \cdot A \cdot t \cdot \int_\lambda L(\lambda)F(\lambda)S(\lambda)\,d\lambda + \xi \tag{8}$$

From the equation (8), it can be seen that the brightness value of a pixel is proportional to integral of the production of the scene's spectral radiance, the filter's spectral transmittance and camera's spectral sensitivity over an interval of wavelength $\lambda$. It is also known from equation (8) that a large aperture (small $f$ number), a large pixel area and a long exposure time all produce a brighter image. But the larger aperture results in a smaller depth of view and the long exposure time blurs the image of dynamic weld pool. The pixel area for a camera is unchangeable.

In the proposed model, only the spectral functions of $L(\lambda)$, $F(\lambda)$ and $S(\lambda)$ are considered while other factors remain the same. So the equation (8) for $G(x)$ is simplified as:

$$G(x) \propto \int_\lambda L(\lambda)F(\lambda)S(\lambda)\,d\lambda \tag{9}$$

By substituting $L(\lambda)$, $F(\lambda)$ and $S(\lambda)$, the integral on the right side of equation (9) is easily calculated by the numerical integration.

While considering the contrast between the weld pool and the arc, the ratio can be calculated as:

$$R_{W/A} = \frac{G_W(x)}{G_A(x)} = \frac{\int_\lambda L_W(\lambda)F(\lambda)S(\lambda)\,d\lambda}{\int_\lambda L_A(\lambda)F(\lambda)S(\lambda)\,d\lambda} = \int_\lambda \frac{L_W(\lambda)}{L_A(\lambda)}F(\lambda)S(\lambda)\,d\lambda \tag{10}$$

where $L_A(\lambda)$ represents the radiation from a small volume in arc column which corresponds a pixel in the image. It is difficult to give the exact spectral distribution for arc radiation, but it is common to think that the arc radiation becomes low with the increase of wavelength in infrared region. So the value of $R_{W/A}$ is smaller in infrared light region, which is better for weld pool imaging.

## 2 Model calculating results

As mentioned in above section, if the spectral radiation of weld pool $L(\lambda)$, the spectral transmittance of filter $F(\lambda)$ and the spectral sensitivity of camera $S(\lambda)$ are giv-

en, the relative brightness of pixel in weld pool image by different filters can be calculated.

The spectral radiation of weld pool $L(\lambda)$ is approximated by the Planck's law, as it does not influence the relative brightness. The temperature of the weld pool is a few hundred degrees higher than the melting point. For steel, the temperature of weld pool is assumed between 1 673 K and 2 073 K. The spectral radiation curves for black body at temperature of 1 673 K, 1 873 K and 2 073 K are predicted by the Planck's Law and shown in Fig. 3.

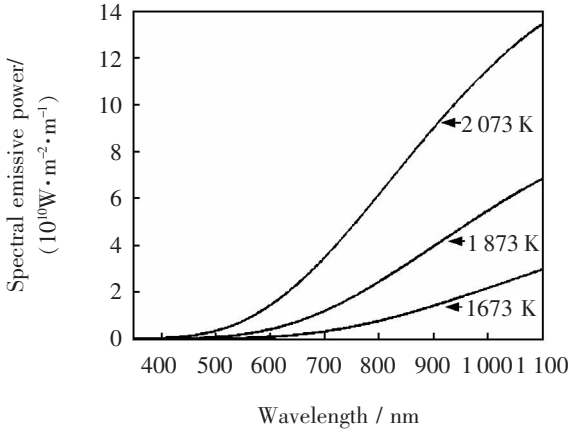


**Fig. 3 Spectral radiance curves at different temperatures predicted by Planck's Law**

When considering the spectral transmittance $F(\lambda)$ for narrow band filter, it can be approximated by Gaussian function using equation (3). In theoretical analysis, only the center wavelengths are different while the peak transmittance $\tau_{max}$ is assumed as 0.5, the FWHM $\Delta\lambda$ is supposed as 10nm and the block range is $[-\infty, \lambda_c - \Delta\lambda) \cup (\lambda_c + \Delta\lambda, +\infty]$, as the practical situation of conventional narrow band filter. So the curve of $F(\lambda)$ for each narrow band filter with different center wavelength can be calculated.

The spectral sensitivity of the camera $S(\lambda)$ used in the experiment is shown in Fig. 4, which is taken from the camera manual. It is shown that the camera is more sensitive to visible light than ultraviolet or infrared light.

Numerical integration of equation (9) is calculated for image brightness of weld pool by narrow band filters with different center wavelengths in range of 360 nm to 1 090 nm. The result is shown in Fig. 5, in which the values are normalized to [0,1]. It is shown that the image brightness of weld pool reaches its maximum with a certain center wavelength in the middle range. And owing to the combined effects of increase of thermal radiation and decrease of the spectral sensitivity in longer wavelength, the center wavelength corresponding to maximum brightness becomes longer when the temperature becomes lower, for example, the center wavelengths are 695nm for 2 073 K, 755 nm for 1 873 K and 788 nm for 1 673 K.

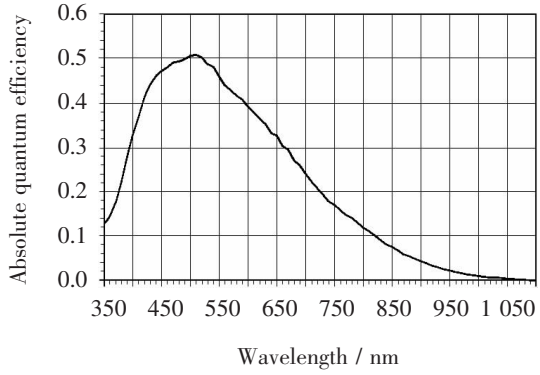


**Fig. 4 Spectral sensitivity curve of Basler camera**

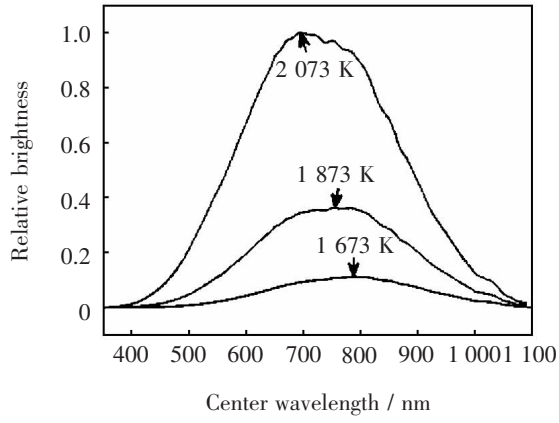


**Fig. 5 Relative brightness calculated for narrow band filters with different center wavelength**

## 3 Experimental results

Bead-on-plate welding experiments were conducted on low carbon steel Q235 of dimension 400 mm × 50 mm × 5 mm. The welding wire material was H08Mn2Si. The diameter of welding wire was 1.2 mm and the wire extension was 18 mm. The shielding gas was 80% Ar + 20%

$CO_2$. The peak current was 400 A, with the voltage of 33 V, and the base current was 50 A with the voltage of 19 V. The frequency of the pulse was 50 Hz. The welding speed was 0.2 m/min. The welding power supply was Fronius TPS2700. During experiments, the workpiece was fixed on a moveable workbench, and the images were captured from rear upper side of the weld pool using the Basler camera with the filter in front of the lens.

In the experiments, 27 narrow band filters with center wavelengths ranging from ultraviolet to infrared range were employed. The characteristic parameters such as center wavelength, FWHM and maximum spectral transmittance for each filter are given in Fig. 6. And for each narrow band filter, the image of weld pool was also shown in Fig. 7.

Comparison between the predicted brightness and the real brightness of weld pool image is made. The predicted relative brightness is calculated using equation (9), in which the temperature is set as 1 773 K and the spectral transmittance for narrow band filter is represented by Gaussian function and the real characteristic parameters. In weld pool image, the brightness of pixels in different regions of weld pool surface is different. The mean brightness values of the weld pool image during the base current period is calculated in a $11 \times 11$ pixels window in the rear region of weld pool excluding the slag. Both of the predicted brightness values by model and the measured brightness values of real image are normalized to make a reasonable comparison. The comparison result is shown in Fig. 7.

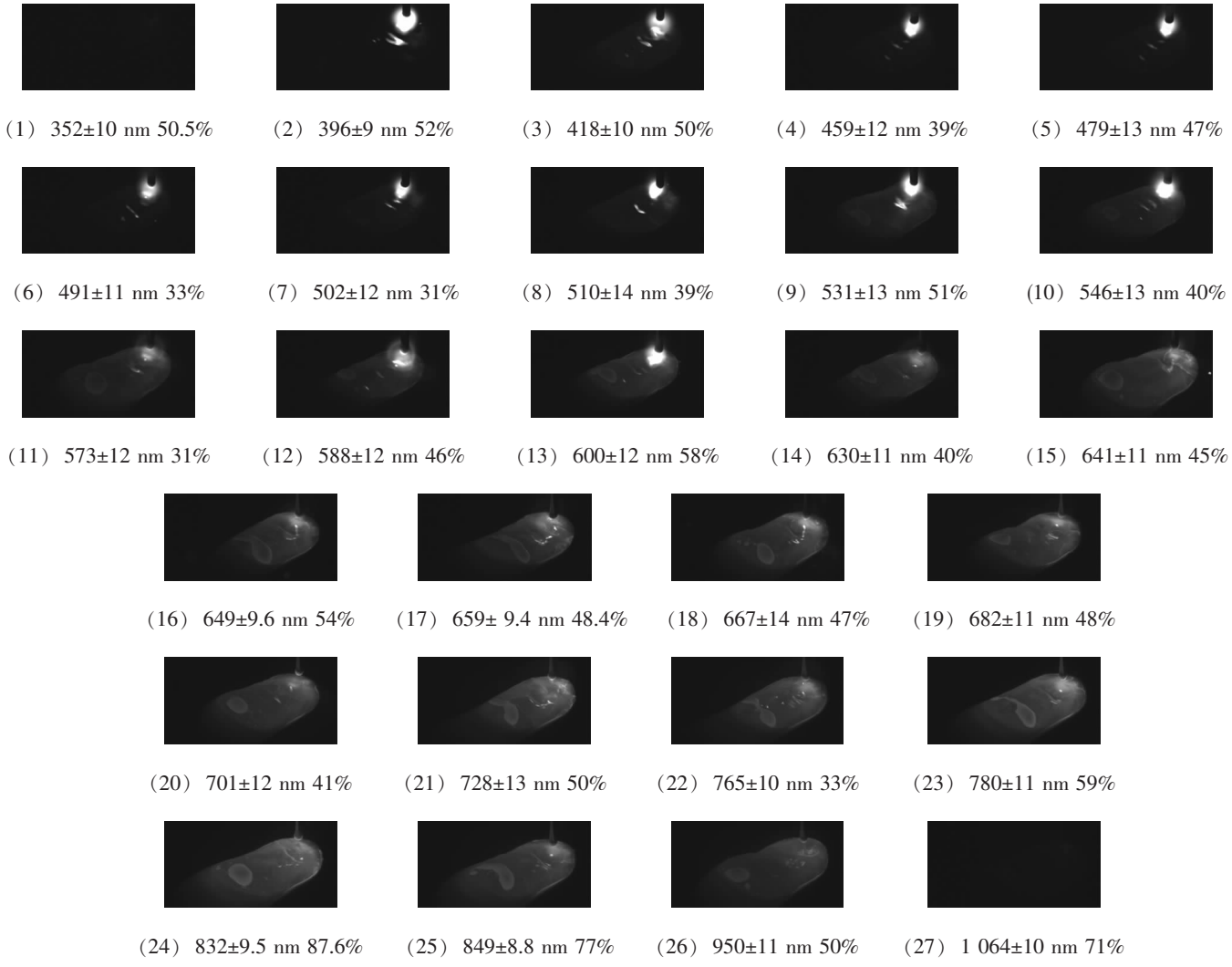


**Fig. 6 Images captured with different narrow band filters**

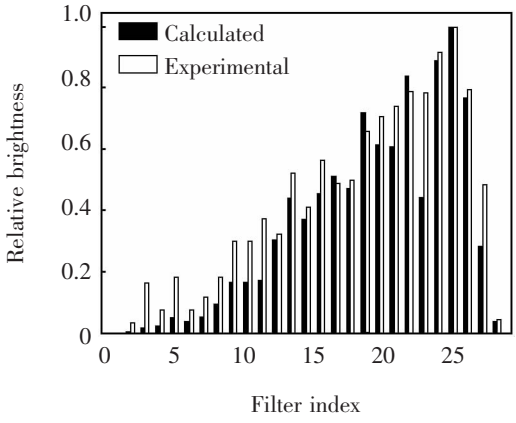


**Fig. 7 Comparison of relative brightness between predicted and measured values**

## 4 Discussion

It has been shown that the relative brightness of weld pool can be predicted by the proposed radiometric model if the radiation of the weld pool, spectral transmittance of the filter and spectral sensitivity of the camera are given. In ideal situations, if only the center wavelength of filter is different while all the other parameters are the same, the brightest image of weld pool can be captured using the filters with center wavelength in the range between 695 nm and 788 nm as shown in Fig. 5. However, in the real situations, the center wavelength, FWHM and the maximum spectral transmittance are different for different narrow filters, but the relative brightness can still be predicted by equation (9). As shown in Fig. 7, the maximum brightness is obtained by the filter of 831 ± 10 nm both in the model predicted values and the measured values. The difference between the predicted value and the measured value for other filters may be caused by errors introduced by the approximated thermal radiation of weld pool and approximated filter spectral transmittance by Gaussian function. Further, the arc is still strong during the base current period and acts like a light source for filters with center wavelengths shorter than 641 nm as shown in Fig. 8. The light emitted from the arc is reflected into the lens by the weld pool surface, so the brightness becomes higher than the predicted one by the model only considering thermal radiation. While in the infrared range, the arc is so weak that almost no light from arc is reflected by the rear section of weld pool, so the predicted value is more accurate.

From Fig. 6 and Fig. 7, it is shown that the characteristic of images captured using different filters are different. During the base current period of P-GMAW, the brightness of the images in weld pool region increases almost monotonously under 831 nm due to the increase of thermal radiation. For filters with center wavelength below 502 nm, the weld pool is dim and the tip of welding wire surrounded by arc is black in the image captured, because the thermal radiation in this interval is too low. Above 531 nm, the boundary and the slag on weld pool surface become discriminable. The slag on the weld pool surface is brighter than the nearby region, which indicates that the radiation of slag is stronger than the molten metal. Over 831 nm, the brightness of weld pool becomes low, especially for the filter of 1 064 ± 10 nm. The reason is that although the radiation is still increasing with wavelength as shown in Fig. 3, but the sensitivity of camera decreases more as shown in Fig. 4. With the narrow band filter of 1 064 ± 10 nm and aperture F8, no weld pool can be seen in the image. The image irradiance must be increased to get a clear image through a larger aperture, longer exposure time or filters with a broader transmitting range. With an enlarged aperture of F1.4 and unchanged exposure time of 250 μs, the captured images are shown in Fig. 8, in which the brightness becomes higher while the boundary is blurred as a result of short depth of view. With aperture F4, legible images of weld pool during peak current period is obtained by the filter of 950 ± 11 nm as shown in Fig. 9. In the experiment, even the fluid flow can be seen by viewing the small particle's movement on the weld pool surface.

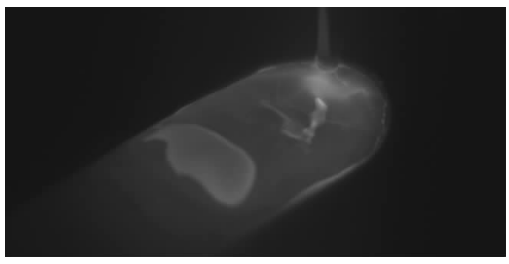

**Fig. 8 Image by filter of 1 064 nm ± 10 nm with aperture F1.4**

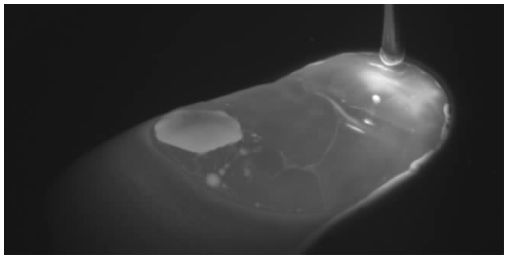

**Fig. 9 Image captured by filter 950 nm ± 11 nm with aperture F4**

## 5 Conclusions

(1) A radiometric imaging model is proposed to predict relative brightness of weld pool by a variety of optical filters considering the spectral thermal radiation, the spectral transmittance of the filter and the spectral sensitivity of the camera. The consistency of the predicted brightness value and measured value verified the effectiveness of the model.

(2) During the base current period of PGMAW for steel, the arc radiation is weak and a clear image of weld pool can be captured by the narrow band filters with center wavelength above 531nm. The maximum image brightness appears when the filter with center wavelength of around 800nm is used .

**Acknowledgement**

The authors are grateful to the financial support for this project from the National Natural Science Foundation of China under grant No. 51205106 and the support from State Key Laboratory of Advanced Welding and Joining, Harbin Institute of Technology.

**References**

[1] Ogawa Y. High speed imaging technique Part 1-high speed imaging of arc welding phenomena. Science and Technology of Welding and Joining, 2011, 16(1): 33 – 43.

[2] Zhao C X, Richardson I M, Kenjeres S, et al. A stereo vision method for tracking particle flow on the weld pool surface. Journal of Applied Physics, 2009,105(12): 123104 – 123108.

[3] Song H S, Zhang Y M. Measurement and analysis of three-dimensional specular gas tungsten arc weld pool surface, Welding Journal, 2008, 87(4): 85s – 95s.

[4] Ma X J, Zhang Y M. Reflection of illumination laser from gas metal arc weld pool surface. Measurement Science and Technology, 2009, 20(11): 280 – 283.

[5] Ma X J, Zhang Y M. Gas metal arc weld pool surface imaging: modeling and processing, Welding Journal, 2011, 90 (5): 85s – 94s.

[6] Kim E W, Allemand C, Eagar T W. Visible light emissions during gas tungsten arc welding and its application to weld image improvement. Welding Journal, 1987, 66(12): 369s – 377s.

[7] Yan Z, Zhang G, Zhang X, et al. Visual sensing and profile extraction of weld pool in pulsed gas metal arc welding. Proceedings of the I MECH E. Part B Journal of Engineering Manufacture, 2004, 218(10): 1333 – 1338.

[8] Inoue K. Image processing for on-line detection of welding process (Report 3) -Improvement of image quality by incorporation of spectrum of arc. Transactions of Joining and Welding Research Institute, 1981,10(1): 13 – 18.

[9] Wang K H, Tang X C, Liu Y, et al. Experimental research on the method of vision detecting MAG welding pool information. Chinese Journal of Mechanical Engineering, 2003, 40 (6): 161 – 164. (in Chinese)

[10] Liu J C. Passive visual sensing in automatic arc welding. Denmark: Technical University of Denmark, 2011.

[11] Liang Z M, Wang D L, Wang J. Vision sensing of P – GMAW weld pool using narrow band filters with different center wavelengths. China Welding, 2013, 22(1): 41 – 46.

[12] Horn B, Sjoberg R W. Calculating the reflectance map. Applied Optics, 1979,18(11) : 1770 – 1779.

[13] Siegel R, Howell J R. Thermal radiation heat transfer (3rd edition). Washington: Hemisphere Publishing Corporation, 1992.

[14] Martinez-Verdu F, Jaume P, Pascual C. Calculation of the color matching functions of digital cameras from their complete spectral sensitivities. Journal of Imaging Science and Technology, 2002, 46(1): 15 – 25.